

FLUX TUBES AT FINITE TEMPERATURE*

NUNO CARDOSO, MARCO CARDOSO, PEDRO BICUDO

CFTP, Departamento de Física, Instituto Superior Técnico
Universidade de Lisboa
Av. Rovisco Pais, 1049-001 Lisbon, Portugal

(Received July 19, 2016)

In this work, we show the flux tubes of the quark–antiquark and quark–quark at finite temperature for SU(3) lattice QCD. The chromomagnetic and chromoelectric fields are calculated above and below the phase transition.

DOI:10.5506/APhysPolBSupp.9.447

1. Introduction

The study of the chromo-fields distributions inside the flux tubes formed by the static $Q\bar{Q}$ and $Q\bar{Q}$ systems are presented in this study. How the flux tube evolves when the distance between quarks or the temperature increase beyond respective critical values are addressed in this paper. In Section 2, we describe the lattice formulation. We briefly review the Polyakov loop for these systems and show how to compute the color fields as well as the Lagrangian distribution. In Section 3, the numerical results are shown. Finally, we conclude in Section 4.

2. Computation of the chromo-fields in the flux tube

The central observables that govern the event in the flux tube can be extracted from the correlation of a plaquette, $\square_{\mu\nu}$, with the Polyakov loops, L ,

$$f_{\mu\nu}(r, x) = \frac{\beta}{a^4} \left[\frac{\langle \mathcal{O} \square_{\mu\nu}(x) \rangle}{\langle \mathcal{O} \rangle} - \langle \square_{\mu\nu}(x) \rangle \right], \quad (1)$$

where $\mathcal{O} = L(0)L^\dagger(r)$ for the $Q\bar{Q}$ system or $\mathcal{O} = L(0)L(r)$ for the QQ system, x denotes the distance of the plaquette from the line connecting

* Presented by N. Cardoso at “Excited QCD 2016”, Costa da Caparica, Lisbon, Portugal, March 6–12, 2016.

quark sources, r is the quark separation, $L(r) = \frac{1}{3} \text{Tr} \prod_{t=1}^{N_t} U_4(r, t)$, where N_t is the number of time slices of the lattice and using the periodicity in the time direction for the plaquette, $\square_{\mu\nu}(x) = \frac{1}{N_t} \sum_{t=1}^{N_t} \square_{\mu\nu}(x, t)$, allows averaging over the time direction.

To reduce the fluctuations of the $\mathcal{O} \square_{\mu\nu}(x)$, we measure the following quantity [1],

$$f_{\mu\nu}(r, x) = \frac{\beta}{a^4} \left[\frac{\langle \mathcal{O} \square_{\mu\nu}(x) \rangle - \langle \mathcal{O} \square_{\mu\nu}(x_R) \rangle}{\langle \mathcal{O} \rangle} \right], \quad (2)$$

where x_R is the reference point placed far from the quark sources.

Therefore, using the plaquette orientation $(\mu, \nu) = (2, 3), (1, 3), (1, 2), (1, 4), (2, 4), (3, 4)$, we can relate the six components in Eq. (2) to the components of the chromoelectric and chromomagnetic fields

$$f_{\mu\nu} \rightarrow \frac{1}{2} (-\langle B_x^2 \rangle, -\langle B_y^2 \rangle, -\langle B_z^2 \rangle, \langle E_x^2 \rangle, \langle E_y^2 \rangle, \langle E_z^2 \rangle) \quad (3)$$

and also calculate the total action (Lagrangian) density, $\langle \mathcal{L} \rangle = \frac{1}{2} (\langle E^2 \rangle - \langle B^2 \rangle)$.

In order to improve the signal over noise ratio, we use the multihit technique [2, 3], replacing each temporal link by its thermal average, and the extended multihit technique [4], which consists in replacing each temporal link by its thermal average with the first N neighbors fixed. Instead of taking the thermal average of a temporal link with the first neighbors, we fix the higher order neighbors, and apply the heat-bath algorithm to all the links inside, averaging the central link

$$U_4 \rightarrow \bar{U}_4 = \frac{\int [\mathcal{D}U_4]_{\Omega} U_4 e^{\beta \sum_{\mu, s} \text{Tr}[U_{\mu}(s)F^{\dagger}(s)]}}{\int [\mathcal{D}U_4]_{\Omega} e^{\beta \sum_{\mu, s} \text{Tr}[U_{\mu}(s)F^{\dagger}(s)]}}. \quad (4)$$

By using $N = 2$, we are able to greatly improve the signal, when compared with the error reduction achieved with the simple multihit. Of course, this technique is more computer intensive than simple multihit, while being simpler to implement than multilevel. The only restriction is $R > 2N$ for this technique to be valid.

3. Results

In this section, we present the results for different β values using a fixed lattice volume of $48^3 \times 8$, Table I. All the computations were done in NVIDIA GPUs using CUDA.

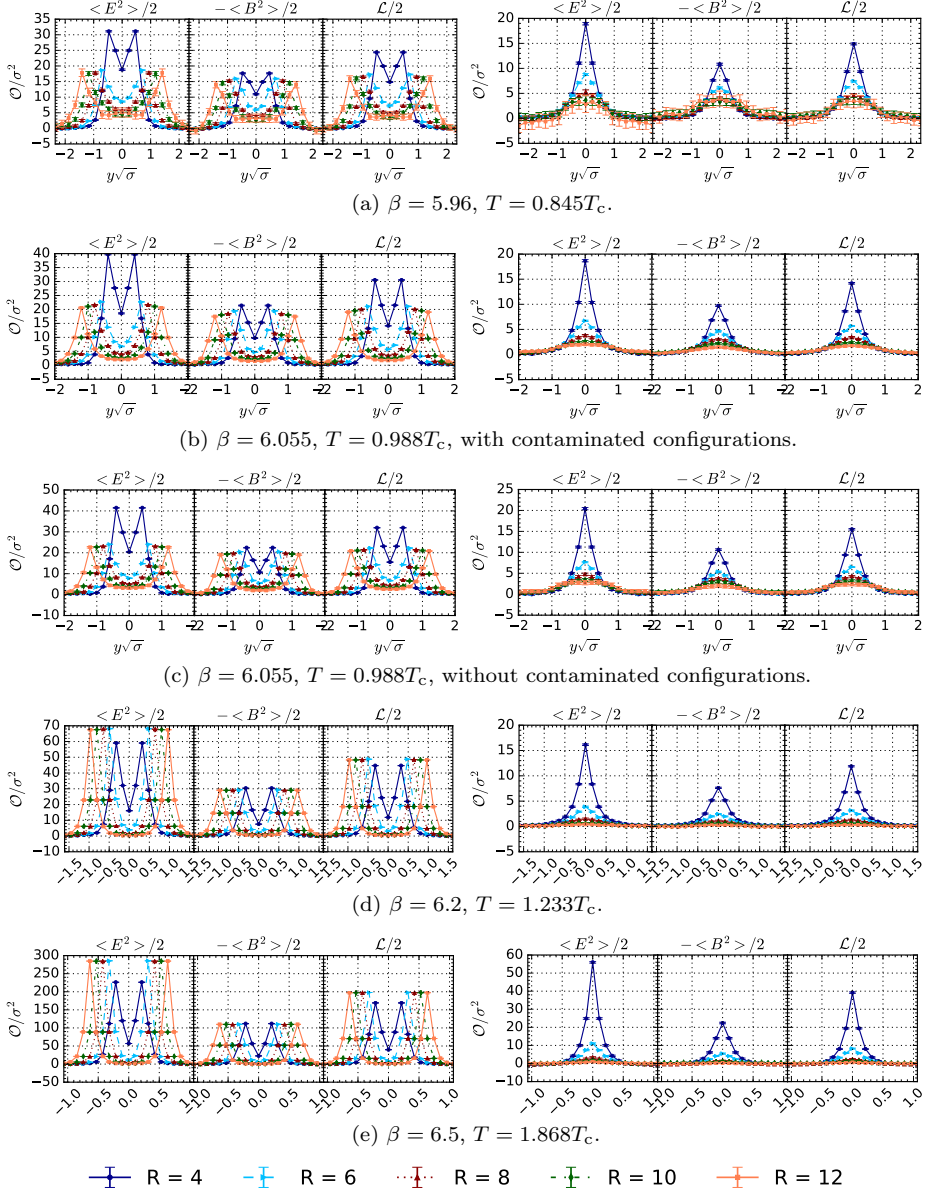


Fig. 1. The results for the $Q\bar{Q}$ system. The results in the left column correspond to the fields along the sources (plane XY) and the right column to the results in the middle of the flux tube (plane XZ). R is the distance between the sources in lattice units.

TABLE I

Lattice simulations for a $48^3 \times 8$ volume. The lattice spacing was computed using the parametrization from [5] in units of the string tension at zero temperature. The * means without configurations in the wrong phase transition.

β	T/T_c	$a\sqrt{\sigma}$	# config.
5.96	0.845	0.235023	5990
6.055	0.988	0.200931	5990/4775*
6.1237	1.100	0.180504	3669
6.2	1.233	0.161013	1868
6.338	1.501	0.132287	3688
6.5	1.868	0.106364	1868

The QQ and $Q\bar{Q}$ are located at $(0, -R/2, 0)$ and $(0, R/2, 0)$ for $R = 4, 6, 8, 10$ and 12 lattice spacing units. In Figs. 1 and 2, we show the results for the $Q\bar{Q}$ system. As expected, the strength of the fields decrease with the temperature. Also, in the confined phase, the width in the middle of the flux tube increases with the distance between the sources, while above the phase transition, the width decreases with the distance.

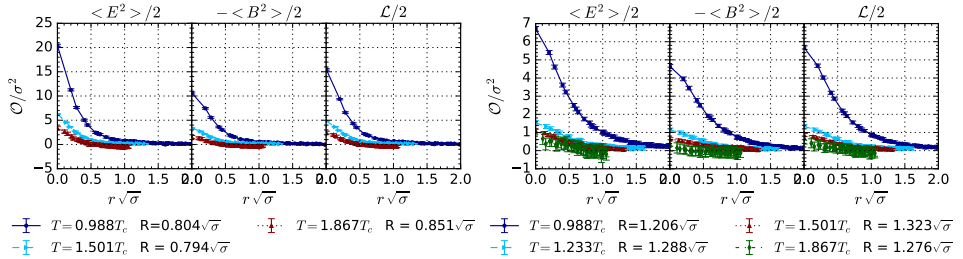


Fig. 2. Results for the fields of the $Q\bar{Q}$ system in the middle of the flux tube in the plane XZ .

Just below the phase transition, $\sim 0.95T_c - 1T_c$, we need to make sure that we do not have contaminated configurations as already mentioned in [6]. By plotting the histogram of Polyakov loop history for $\beta = 6.055$ ($T = 0.988T_c$), Fig. 3, we observe a double peak structure, this means that the configurations that lie on the second peak correspond to configurations on the wrong phase and, therefore, we need to remove this configurations from the statistics. Therefore, in Table I, the value with asterisk corresponds to the configurations after removing these contaminated configurations. In Figs. 4 (a) and 4 (b), we show the results of this effect for the QQ system below the phase transition. In Fig. 5, we compare the results for the $Q\bar{Q}$ and QQ systems above the phase transition. As expected, the results are in agreement.

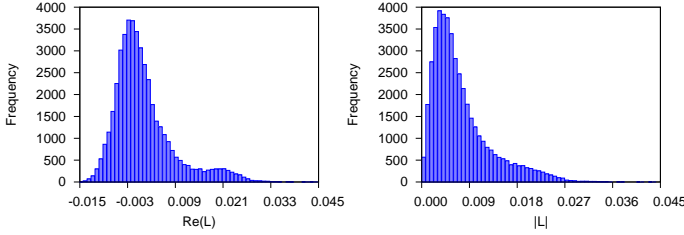


Fig. 3. Histogram of the Polyakov loop history for $\beta = 6.055$.

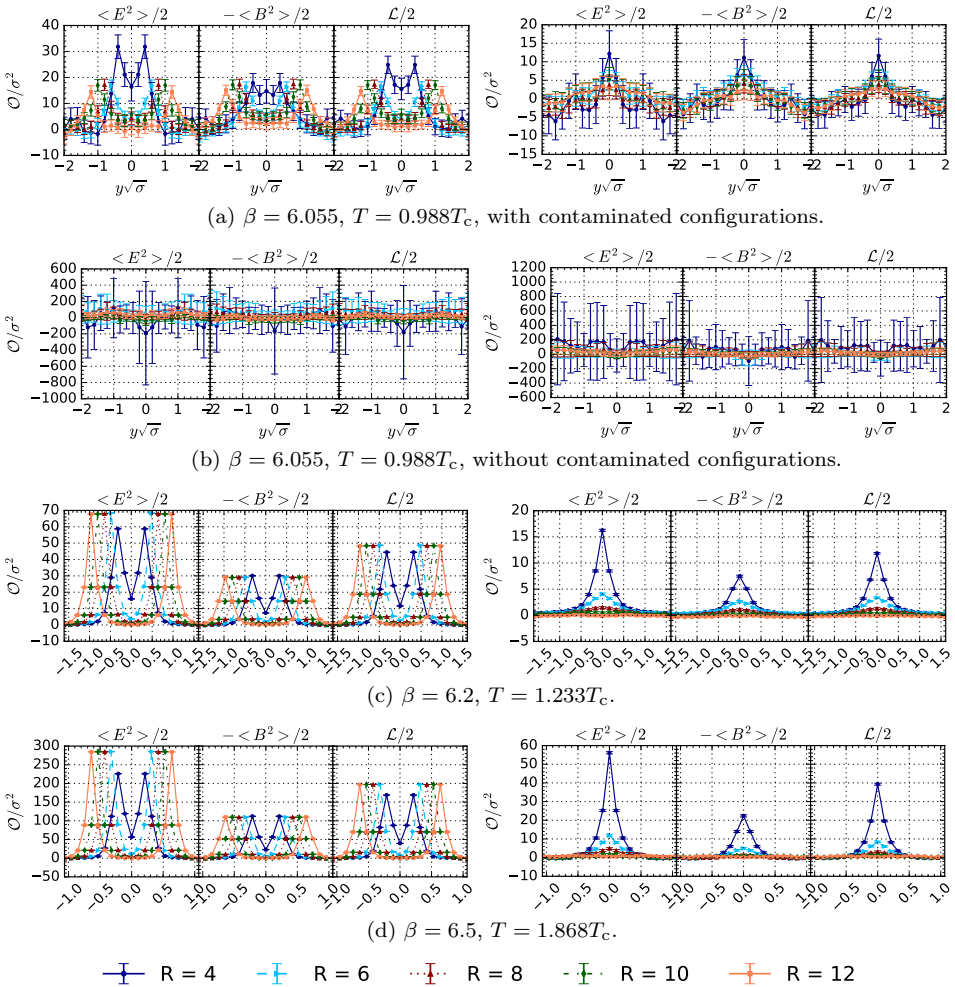


Fig. 4. The results for the QQ system. The results in the left column correspond to the fields along the sources (plane XY) and the right column to the results in the middle of the flux tube (plane XZ). R is the distance between the sources in lattice units.

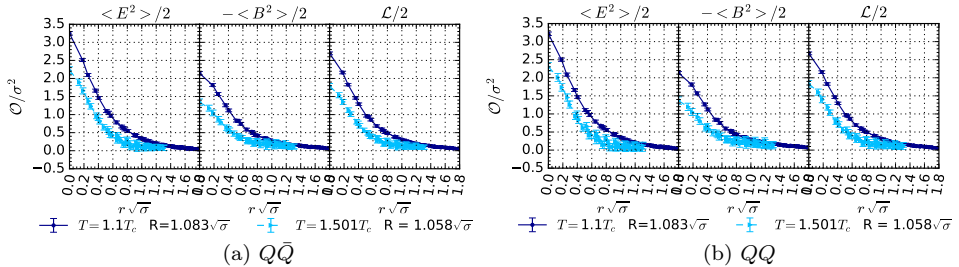


Fig. 5. Results for the fields in the middle of the flux tube in the plane XZ .

4. Conclusions

As the distance increases between the sources, the field strength at the flux tube decreases as already seen in studies at zero temperature. Below the phase transition, the fields strength decreases as the temperature increases. However, above the phase transition, the fields rapidly decrease to zero as the quarks are pulled apart. The width of the flux tube below the phase transition increases with the separation between the quark–antiquark, however above the phase transition the width seems to decrease.

Nuno Cardoso and Marco Cardoso are supported by FCT under the contracts SFRH/BPD/109443/2015 and SFRH/BPD/73140/2010 respectively. We also acknowledge the use of CPU and GPU servers of PtQCD, supported by NVIDIA, CFTP and FCT grant UID/FIS/00777/2013.

REFERENCES

- [1] Y. Peng, R.W. Haymaker, *Phys. Rev. D* **47**, 5104 (1993).
- [2] R. Brower, P. Rossi, C.-I. Tan, *Nucl. Phys. B* **190**, 699 (1981).
- [3] G. Parisi, R. Petronzio, F. Rapuano, *Phys. Lett. B* **128**, 418 (1983).
- [4] N. Cardoso, M. Cardoso, P. Bicudo, *Phys. Rev. D* **88**, 054504 (2013).
- [5] R.G. Edwards, U.M. Heller, T.R. Klassen, *Nucl. Phys. B* **517**, 377 (1998).
- [6] N. Cardoso, P. Bicudo, *Phys. Rev. D* **85**, 077501 (2012).